

## Metallic conductivity near the metal-insulator transition in $\text{Cd}_{1-x}\text{Mn}_x\text{Te}$

C. Leighton and I. Terry

*Department of Physics, University of Durham, Science Laboratories, South Road, Durham, DH1 3LE, United Kingdom*

P. Becla

*Department of Materials Science and Engineering, Massachusetts Institute of Technology, Cambridge, Massachusetts 02139*

(Received 2 February 1998)

The low-temperature transport properties of the diluted magnetic semiconductor  $\text{Cd}_{1-x}\text{Mn}_x\text{Te}:\text{In}$  (or  $\text{In}$ ,  $\text{Al}$ ) have been studied on the metallic side of the metal-insulator transition (MIT). The critical region near the MIT has been probed by utilizing the persistent photoconductivity effect displayed by this material. This has allowed us to study the MIT in a single sample of this magnetic semiconductor in zero magnetic field. The critical behavior is consistent with the predictions of the scaling theory of electron localization with a conductivity critical exponent close to 1.0. The critical carrier density is determined to be  $2.3 \times 10^{17} \text{ cm}^{-3}$  for  $x = 0.08$ . The temperature dependence of the metallic conductivity in the critical region (below 1 K) is well described by a theory that takes into account the effects of  $e^-e^-$  interactions and weak localization. The transport properties of  $\text{Cd}_{1-x}\text{Mn}_x\text{Te}:\text{In}$  and  $\text{Cd}_{1-x}\text{Mn}_x\text{Te}:\text{In, Al}$  have been studied in the weakly localized regime. At low temperatures the samples with low Mn content ( $x \leq 0.06$ ) display a rapid decrease of the conductivity below a certain temperature. This effect (which has previously been observed in  $\text{Cd}_{1-x}\text{Mn}_x\text{Se}$ ) is due to the scattering of electrons by bound magnetic polarons (BMP's) formed on quasilocalized  $s$  spins. However, in samples with higher  $x$ , we observe no evidence for this form of scattering. We propose that such an effect is only observable in the paramagnetic phase, whereas, in the presence of spin-glass order, the temperature dependence of the BMP scattering process is weak enough to be masked by other electron scattering mechanisms. [S0163-1829(98)00439-1]

### I. INTRODUCTION

In recent years, experimental studies of the metal-insulator transition (MIT) have attempted to elucidate the behavior of the conductivity in the critical region, in order to test the newly developed scaling theory of electron localization.<sup>1</sup> The scaling theory, which was born from the Anderson localization concept,<sup>2</sup> predicts that the MIT is a continuous phase transition with the conductivity of doped semiconductors having the following critical form:

$$\sigma(T=0, n) = \sigma_0(n/n_c - 1)^v, \quad (1)$$

where  $n$  is the carrier density,  $n_c$  is the critical value of the carrier density, and  $v$  is the conductivity critical exponent.

Materials such as  $\text{Si:P}$ ,<sup>3</sup>  $\text{Si:As}$ ,<sup>4</sup> and  $\text{Ge:As}$  (Ref. 5) have been studied by growing sets of samples with various dopant densities and measuring the temperature dependence of the conductivity at very low temperature. This allows an extrapolation to absolute zero and a test of Eq. (1). In general, experiments on uncompensated semiconductors seem to result in an exponent close to 0.5, while compensated semiconductors display  $v \approx 1.0$ .<sup>6</sup> A conductivity exponent of 1.0 is in agreement with scaling theory with  $e^-e^-$  interactions taken into account, whereas the exponent close to 0.5 found in Ref. 3, for example, is difficult to reconcile with theoretical predictions.<sup>7</sup>

Although measurements such as these have resulted in the determination of the conductivity exponent in a wide variety of systems, it is advantageous to be able to continuously "fine-tune" the transition via a controllable parameter. For

example, in  $\text{Si:P}$  this has been achieved by the application of stress,<sup>8</sup> resulting again in an exponent of 0.5. Another method of fine tuning the MIT is to use the persistent photoconductivity (PPC) effect exhibited by certain semiconductors. Here the conductivity and carrier density show an increase on illumination, which persists after the illumination ceases. The MIT has been studied in this fashion in the  $DX$  center<sup>9</sup> persistent photoconductor  $\text{Al}_x\text{Ga}_{1-x}\text{As}:\text{Si}$ ,<sup>10</sup> where an exponent of 1.0 was deduced, both in zero magnetic field and in an applied field of 4 T. It should be noted that one of the major advantages of fine-tuning techniques such as the use of PPC, is that measurements can be made very close to criticality.

The MIT has also been studied in magnetic (and diluted magnetic) semiconductors. In materials such as  $\text{Gd}_{3-x}\text{V}_x\text{S}_4$ ,<sup>11</sup>  $\text{Cd}_{1-x}\text{Mn}_x\text{Se}$ , and  $\text{Hg}_{1-x}\text{Mn}_x\text{Te}$  (Ref. 12) magnetic field can be used to fine-tune the transition. In each of these cases, the conductivity exponent was found to be close to 1.0, in agreement with the scaling theory with interactions. It should be noted that the application of magnetic field can complicate the situation somewhat in that it is possible that the fields required to induce a transition will result in a crossover to a high-field or spin-polarized<sup>12</sup> universality class. In this paper, we present the results of a study of the MIT in a diluted magnetic semiconductor using the PPC technique. This provides a unique opportunity to study the MIT critical region in zero magnetic field in a magnetic system. The PPC effect in  $\text{Cd}_{1-x}\text{Mn}_x\text{Te}:\text{In}$  (which is due to the formation of  $DX$  centers) is discussed in detail elsewhere.<sup>13,14</sup>

As well as a study of the MIT in  $\text{Cd}_{1-x}\text{Mn}_x\text{Te}:\text{In}$ , this paper also reports measurements on the temperature depen-

TABLE I. Summary of the transport data for the sample used in this study. The Mn concentration, conductivity at 300 K, conductivity at 4.2 K, carrier density at 300 K, mobility at 300 K, proximity to the MIT, and dopants are shown.

Sample	$x$	$\sigma(300\text{ K})$ [( $\Omega\text{ cm}$ ) <sup>-1</sup> ]	$\sigma(4.2\text{ K})$ [( $\Omega\text{ cm}$ ) <sup>-1</sup> ]	$n(300\text{ K})$ (10 <sup>17</sup> cm <sup>-3</sup> )	$\mu(300\text{ K})$ (cm <sup>2</sup> V <sup>-1</sup> s <sup>-1</sup> )	Proximity to MIT	Dopant
A1	4.7±0.2	21.74	9.71	3.0	453	WLR	In
A2	6.1±0.2	19.23	7.94	2.3	523	WLR	In
A5	8.1±0.3	6.45	0.19	2.0	202	tunable	In
C5	8.1±0.2	6.45	0.21	2.0	202	tunable	In
INAL4	18.1±0.3	4.10	0.37	3.98	85.2	critical	In, Al

dence of the conductivity in the weakly localized regime (WLR) at low temperatures. Previous measurements of the transport properties of Cd<sub>0.95</sub>Mn<sub>0.05</sub>Se:In in this region have indicated that the magnetic properties of the system have a large effect on the conductivity.<sup>15</sup> Specifically, the ferromagnetic  $s$ - $d$  exchange interaction leads to the formation of magnetic excitations known as bound magnetic polarons (BMP's). Here, the  $s$ - $d$  exchange interaction polarizes the  $S = \frac{5}{2}$  Mn spins within the Bohr radius of a donor electron. This results in a ferromagnetic cloud of aligned Mn spins, which has a very large low-field magnetic susceptibility. In the WLR in Cd<sub>0.95</sub>Mn<sub>0.05</sub>Se:In the conductivity is seen to exhibit a rapid and unexpected drop below about 0.5 K. This was interpreted by Dietl *et al.*<sup>15</sup> in terms of polaron formation on quasilocalized  $s$  spins, which have been postulated to exist in the WLR. The polarons result in an added contribution to the spin-disorder scattering rate, which leads to a rapid drop in the conductivity upon reducing the temperature below the point at which the  $s$ - $d$  exchange interaction dominates over thermal fluctuations. This hypothesis was backed up by the results of a calculation in which the effect of temperature on the Bohr radius of the polaron was used to model the temperature dependence of the conductivity. In addition to this, a direct calculation of the spin-disorder scattering rate due to the polaron formation was found to be in excellent agreement with the experimental data.

BMP formation is also seen to dominate the transport properties of Cd<sub>1-x</sub>Mn<sub>x</sub>Te:In on the insulating side of the transition.<sup>16</sup> In particular, polaron formation can lead to a magnetic hard gap in the density of states.<sup>16</sup> In this situation an activated form for the conductivity,  $\exp[-(E_H/k_B T)]$ , where  $E_H$  is the hard-gap width, is observed in zero magnetic field. When a magnetic field of 8 T is applied the activated form for the conductivity is lost and the temperature dependence is consistent with the Efros-Shklovskii form for variable range hopping (VRH) with  $e^-$ - $e^-$  interactions included. This is due to the fact that the binding energy of the BMP's is reduced to zero by the application of a magnetic field, as the difference in magnetization between the background Mn spins and the polarons is zero when the background spins are aligned with the field. Finally, it is worth noting that the BMP formation also dominates the magnetotransport<sup>17</sup> and (persistent) photomagnetization<sup>18</sup> in these materials.

This paper is organized as follows. Sec. II describes the samples used in this study along with the experimental arrangement and techniques. In Sec. III the results of the PPC fine-tuning experiment are presented, and the temperature

dependence of the metallic conductivity near  $n_c$  is examined quantitatively. Sec. IV contains the results of the experiments on the WLR of Cd<sub>1-x</sub>Mn<sub>x</sub>Te, where the BMP scattering is observed in some samples. A summary of the work and a set of conclusions is presented in Sec. V.

## II. SAMPLES AND EXPERIMENT

The bulk samples of Cd<sub>1-x</sub>Mn<sub>x</sub>Te that were used in this study were grown by the vertical Bridgman technique. Doping is with indium or both indium and aluminum. In the samples of Cd<sub>1-x</sub>Mn<sub>x</sub>Te:In, the doping level is typically in the 10<sup>18</sup>-10<sup>19</sup> cm<sup>-3</sup> range, which results in all of the samples being  $n$  type. Heavy compensation occurs due to the existence of Cd vacancies introduced during the growth, although post-growth annealing in Cd vapor can produce samples with free electron densities large enough to study the MIT. Despite this, it is very difficult to find samples in which it is possible to illuminate from the insulating to metallic phase. The composition of the samples is determined quite accurately by energy dispersive analysis of x-Rays (EDAX). This information is shown in Table I along with a summary of the transport data for these samples.

Before preparation for the electrical measurements the samples were checked for compositional homogeneity by inspection with an infrared microscope. Some samples were also examined in a scanning electron microscope where the spatial variations in composition can be analyzed quantitatively using the EDAX technique. The compositional fluctuations were found to be rather small.<sup>14</sup> Samples are prepared for the electrical measurements by first polishing to a finish of about 1  $\mu\text{m}$ , and then etching in a 3% Br in CH<sub>3</sub>OH solution for periods of about 1 min. Ohmic electrical contacts are made by immediately soldering 50- $\mu\text{m}$ -diameter Au wires to the perimeter of the surface of the sample in a van der Pauw configuration. Clean, high purity (99.9999%) indium is used as a contact material.

The transport measurements at <sup>4</sup>He temperatures and above were performed using standard dc techniques, with the sample well thermally anchored in a continuous flow cryostat that was situated between the pole pieces of an electromagnet capable of 0.75 T. The sample temperature can be accurately measured and controlled (to <0.1 K) from 360 K down to 3.9 K. The low-temperature measurements were performed in a sorption pumped <sup>3</sup>He system, down to  $\approx$ 300 mK. The temperature of the sample in this system is measured using a RhFe sensor above 1.4 K and a Speer resistor below 1.4 K. Great care is taken to ensure that the samples,

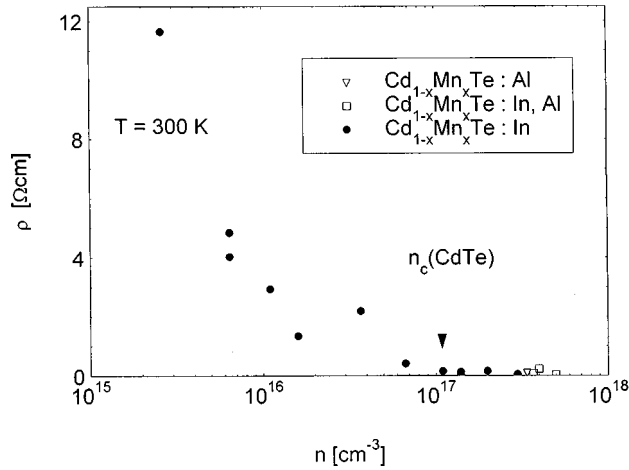


FIG. 1. Resistivity against carrier density at 300 K for several samples of  $\text{Cd}_{1-x}\text{Mn}_x\text{Te}$ . The critical carrier density of CdTe is shown to give an indication of where the MIT occurs.

which are mounted on sapphire wafers and attached to the  $^3\text{He}$  pot with high thermal conductivity varnish, remain in good thermal contact with the thermometer and pot. Ample time is allowed for equilibration at each temperature, while regular checks for sample self-heating are carried out by measuring  $V$ - $I$  curves at low temperatures. The effect of self-heating is reduced to a negligible level by the use of currents down to 100 nA, which result in dissipated power levels of  $10^{-11}$  W.

The sample illumination in all cases is provided by a Kodenshi  $\text{Al}_x\text{Ga}_{1-x}\text{As}$  infrared light emitting diode (LED), with a peak emission intensity at 940 nm. This LED is wired in series with a 1 k $\Omega$  resistor to allow the current in the circuit (and hence the emission intensity) to be controlled by varying the applied voltage. At  $^3\text{He}$  temperatures the illumination can be pulsed to avoid heating effects.

### III. THE MIT IN $\text{Cd}_{1-x}\text{Mn}_x\text{Te:In}$

A plot of the 300 K resistivity against carrier density (as determined by Hall measurements) is shown in Fig. 1, for a number of samples of  $\text{Cd}_{1-x}\text{Mn}_x\text{Te}$ , with various compositions. As expected, the resistivity shows a rapid decrease with increasing carrier density. The critical carrier density of CdTe is shown to give an indication of where the MIT occurs. As noted in a previous paper,<sup>14</sup> the value of  $n_c$  in  $\text{Cd}_{1-x}\text{Mn}_x\text{Te}$  is dependent on the value of  $x$ , as the Bohr radius of the donors changes with composition. The critical density can be estimated from the Mott criterion,<sup>19</sup>

$$n_c = \left( \frac{0.26}{a_H} \right)^3, \quad (2)$$

where  $a_H$  is the effective Bohr radius of the donor. For CdTe this results in  $n_c \approx 1.1 \times 10^{17} \text{ cm}^{-3}$ . In  $\text{Cd}_{1-x}\text{Mn}_x\text{Te:In}$ , the value of  $a_H$  is expected to decrease with increasing  $x$  leading to an increase in the critical density. Unfortunately, the values of the static dielectric constant and the effective mass required to calculate  $a_H$ , and therefore  $n_c$ , are unknown for zinc-blende MnTe. Experimentally,  $n_c$  has been estimated to be  $\sim 2 \times 10^{17} \text{ cm}^{-3}$  for  $x=0.05$ .<sup>20</sup> In addition to this, mea-

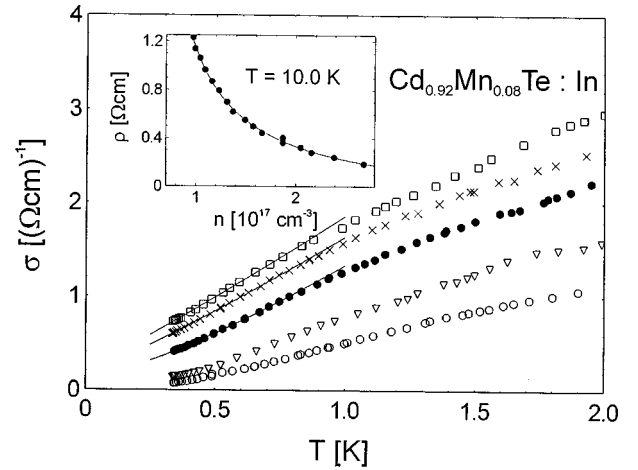


FIG. 2. Temperature dependence of the conductivity of  $\text{Cd}_{0.92}\text{Mn}_{0.08}\text{Te:In}$  from 2 K down to 335 mK. Five photogenerated carrier densities are shown: 2.17, 2.33, 2.61, 2.69, and  $2.77 \times 10^{17} \text{ cm}^{-3}$ . The solid lines are fits to Eq. (3) with the parameters in Table II. The inset shows the calibration curve of resistivity against carrier density at 10.0 K. Here the solid line is a guide to the eye.

surements in the insulating phase by Terry *et al.* suggest  $n_c \approx 2.3 \times 10^{17} \text{ cm}^{-3}$  for  $x=0.09$ .<sup>16</sup>

The low-temperature conductivity of a sample of  $\text{Cd}_{0.92}\text{Mn}_{0.08}\text{Te:In}$ , which can be illuminated from the insulating to metallic phase (sample C5), is shown in Fig. 2. Each curve in this figure corresponds to a different photogenerated carrier density in the range  $2.17 \times 10^{17}$  to  $2.77 \times 10^{17} \text{ cm}^{-3}$ . These values of the carrier density are determined from the resistivity at 10 K using the calibration curve shown in the inset of this figure. These data are obtained by illuminating the sample in stages, removing the illumination, and measuring the Hall coefficient and resistivity at a fixed temperature of 10.0 K. It should be noted that more curves were measured, but only five are presented for the purposes of clarity.

The data of Fig. 2 clearly indicate that we are observing a MIT in this system; the low-carrier density curves result in a zero value for the conductivity at absolute zero, whereas the higher-carrier density curves would appear to indicate a finite value of the conductivity extrapolated to absolute zero. Further evidence for this conclusion is provided by the fact that the form of the temperature dependence of the conductivity is quantitatively different for the low- and high-carrier density curves. The lowest-carrier density curve ( $2.17 \times 10^{17} \text{ cm}^{-3}$ ) actually displays a temperature dependence of the conductivity, which is consistent with Efros-Shklovskii VRH,<sup>21</sup> indicating that this curve corresponds to insulating conduction. The higher-carrier density curves can be fitted with a form for the temperature dependence of the conductivity, which includes corrections to the finite  $T=0$  conductivity due to  $e^-e^-$  interactions, and weak localization. This model (which results in the fits shown by the solid lines in Fig. 2) is described in detail below.

The behavior of the conductivity in the critical region of the MIT is shown in Fig. 3, where the low-temperature conductivity is plotted as a function of the Hall carrier density. This plot is used as an approximation to the behavior of the

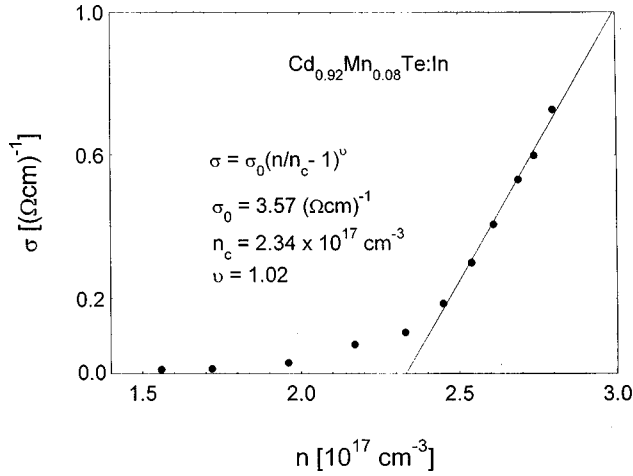


FIG. 3. Critical behavior of the low-temperature conductivity.  $T=335$  mK. The solid line is a fit to the scaling form (1), with the parameters shown in the figure.

zero-temperature conductivity, as an extrapolation to absolute zero from 300 mK can lead to ambiguous results. It should be noted that this procedure has been used successfully in the past.<sup>1</sup> Although thermal rounding effects are present it seems clear that we are observing a continuous MIT in this system. Moreover, beyond the thermally rounded region the  $n$  dependence of the low-temperature conductivity is consistent with the scaling-theory prediction for the critical behavior. The solid line is a fit to Eq. (1) with  $\sigma_0 = 3.57 \pm 0.35 (\Omega \text{ cm})^{-1} = 0.71 \sigma_{\min}(\text{CdTe})$ ,  $n_c = (2.34 \pm 0.25) \times 10^{17} \text{ cm}^{-3}$ , and  $\nu = 1.02_{-0.15}^{+0.18}$ . An exponent close to 1.0 is in agreement with past work on magnetic semiconductors in finite magnetic fields, as well as the scaling theory with  $e^-e^-$  interactions included. It should also be noted that, as mentioned earlier, the vast majority of compensated semiconductors exhibit  $\nu \approx 1.0$  and this material is indeed heavily compensated (we estimate  $0.7 < K < 0.97$ , where  $K$  is the compensation ratio). The value of the critical carrier density  $n_c$  of  $2.34 \times 10^{17} \text{ cm}^{-3}$  would appear to be in reasonable agreement with the work of Shapira *et al.* on the magnetoresistance in  $\text{Cd}_{1-x}\text{Mn}_x\text{Te:In}$  ( $n_c \approx 2.0 \times 10^{17} \text{ cm}^{-3}$  for  $x = 0.05$ ) (Ref. 20) and Terry *et al.* ( $n_c \approx 2.3 \times 10^{17} \text{ cm}^{-3}$  for  $x = 0.09$ ).<sup>16</sup>

The value of the conductivity prefactor  $\sigma_0$  is also of some interest. Work on Si:P,<sup>3</sup> as well as many other materials, results in a value for  $\sigma_0$  that is well in excess of the estimated minimum metallic conductivity, whereas this work suggests that the conductivity prefactor for  $\text{Cd}_{1-x}\text{Mn}_x\text{Te:In}$  is less than the value of  $\sigma_{\min}$ . The value of  $\sigma_{\min}$  can be calculated from the Mott expression,<sup>19</sup>  $\sigma_{\min} = Ce^2/\hbar a$ , where  $C \approx 0.03$  and  $a$  is the mean distance between electrons. Of course, the value of  $\sigma_{\min}$  for  $\text{Cd}_{1-x}\text{Mn}_x\text{Te:In}$  is bigger than the value for CdTe due to the reduction in the size of  $a$ . This reduction in  $a$  from  $x=0$  to  $x=0.08$  can be estimated from the measured value of  $n_c$  at  $x=0.08$  and the value of  $1.1 \times 10^{17} \text{ cm}^{-3}$  at  $x=0.0$ . This calculation leads to  $\sigma_{\min}(x=0.08) = 6.4 (\Omega \text{ cm})^{-1}$ , giving  $\sigma_0 = 0.56 \sigma_{\min}$ .

To investigate the question regarding the relative size of the conductivity prefactor and the minimum metallic conductivity further, the values for  $\sigma_0$  and  $\sigma_{\min}$  for a variety of systems are plotted in Fig. 4 as  $\sigma_0/\sigma_{\min}$  against  $\sigma_{\min}$ . It

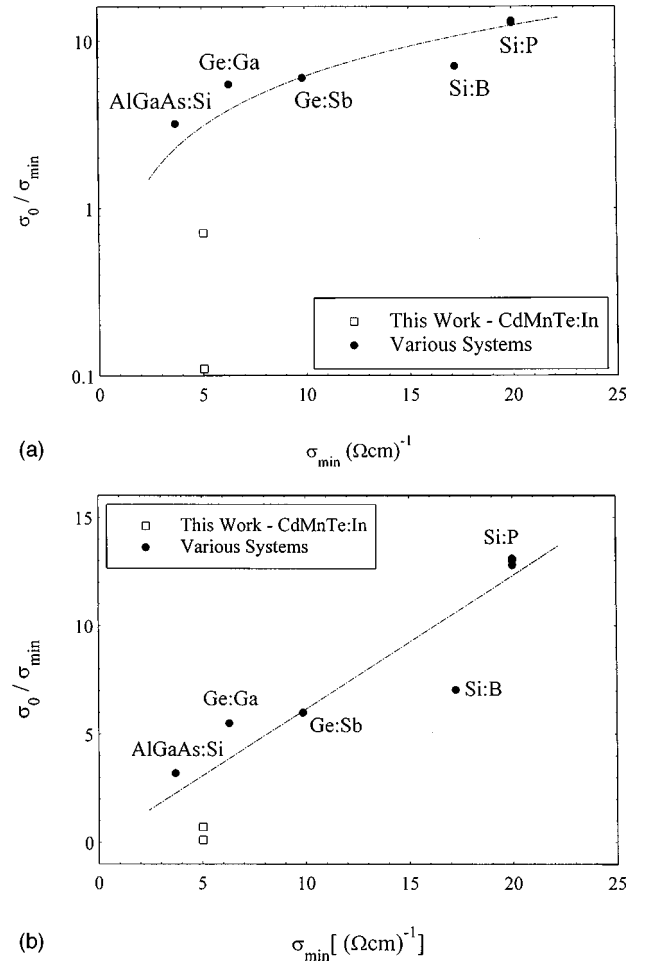


FIG. 4. Plot of  $\sigma_0/\sigma_{\min}$  against  $\sigma_{\min}$  for various materials. The dashed line is a guide to the eye.

seems clear that  $\sigma_0/\sigma_{\min}$  is a material-dependent quantity. An interesting trend is observed, with the largest ratios of the conductivity prefactor to the minimum metallic conductivity occurring for materials with large values of the minimum metallic conductivity, and hence small values of the Bohr radius.

The temperature dependence of the conductivity in the metallic phase (see Fig. 2) can be adequately described by the following expression:<sup>22</sup>

$$\sigma(n, T) = \sigma_0 + m(n)T^{1/2} + B(n)T^{p/2}, \quad (3)$$

which has been applied to doped semiconductors before.<sup>23,24</sup> Here, the first term is the conductivity at  $T=0$ , the second term is a correction due to the effects of  $e^-e^-$  interactions, and the third term is a correction for the effects of weak localization. Dealing with the  $mT^{1/2}$  term first we have<sup>22</sup>

$$m = \alpha \left[ \frac{4}{3} - \left( \frac{3}{2} \gamma F_\sigma \right) \right], \quad (4)$$

where

$$\alpha = \frac{e^2}{\hbar} \left( \frac{1.3}{4\pi^2} \right) \left( \frac{k_B}{2\hbar D} \right)^{1/2}. \quad (5)$$

TABLE II. The fitting parameters deduced from conductivity data and Eq. (3). The data are listed for sample C5 (data in Fig. 2) and another sample, A5. The two values of  $B$  quoted are the experimentally determined value and the value calculated from Eq. (6).

Sample	$n/n_c$	$m$ [[ $\Omega$ cm $K^{1/2}$ ] $^{-1}$ ]	$\gamma F_\sigma$	$B_{\text{expt.}}$ [[ $\Omega$ cm $K$ ] $^{-1}$ ]	$B_{\text{theory}}$ [[ $\Omega$ cm $K$ ] $^{-1}$ ]
C5	1.183	-1.90	1.148	3.08	1.74
C5	1.149	-1.85	1.138	2.66	1.73
C5	1.115	-1.65	1.108	2.49	1.70
A5	1.309	-2.57	1.167	2.73	2.08
A5	1.233	-2.20	1.123	2.30	2.06
A5	1.177	-1.41	1.037	1.61	2.05

In these expressions,  $D$  is the diffusion coefficient and  $\gamma F_\sigma$  is the Coulomb interaction parameter where  $\gamma$  is a constant that can be calculated from the band structure. The quantity  $F_\sigma$  is then related to the Fermi-liquid parameter,  $F$  by

$$F_\sigma = (-32/3) \left[ 1 - \frac{3F}{4} - \left( 1 - \frac{F}{2} \right)^{3/2} \right] F^{-1}.$$

Now, considering the second term in Eq. (3), we have  $\tau_\phi^{-1} = cT^p$ , where  $\tau_\phi$  is the relaxation time of the dominant dephasing mechanism,  $c$  is a constant, and the exponent  $p$  is a constant that depends on the details of the dephasing mechanism. For  $e^-e^-$  scattering in the clean limit as the dominant mechanism theory predicts  $p=2$ ,<sup>22</sup> whence  $B(n)$  is given by<sup>23</sup>

$$B(n) = \frac{e^2}{\hbar \pi^2} \left[ \frac{S_0 \eta}{2} \left( \frac{c}{D} \right)^{1/2} \right], \quad (6)$$

where  $\eta$  is the valley degeneracy and  $S_0$  is a constant that can be calculated from the effective-mass anisotropy and the value of  $\eta$ . Note that the situation for CdTe is simplified by the fact that  $S_0 \eta = 1.0$ .

Preliminary fits to the data of Fig. 2 established immediately that good agreement can only be obtained when  $p$  is close to 2.0. The value of  $p$  was therefore set at 2.0 and the fitting procedure repeated with  $m$ ,  $B$ , and  $\sigma(n, T=0)$  as fitting parameters. As can be seen from the figure, this results in good agreement below 1 K, with the parameters shown in Table II. The determined values of  $m(n)$  were used to calculate the quantity  $\gamma F_\sigma$  as shown in the table. The values of the diffusion coefficient required to do this are calculated from the transport data using the Einstein relations. A trend of increasing  $\gamma F_\sigma$  with increasing  $n$  is observed, as was the case in Si:B.<sup>24</sup> However, unlike the data for Si:B, the values of  $\gamma F_\sigma$  are rather close to 1.0. Combining this with the fact that  $\gamma F_\sigma$  shows a tendency to saturate as  $n$  is increased, suggests that the constant  $\gamma$  is close to unity. It should be noted that the determined values of  $m$  are of the same order of magnitude as found in a variety of systems.<sup>4,23,24</sup>

Following Thomas *et al.*,<sup>23</sup> it is possible to calculate the theoretical predictions for the parameter  $B(n)$ . These values are also shown in Table II, along with the values deduced from the fits to the experimental data. Although the agreement is not exact, the values agree to within a factor of 2. Again, the values of  $B$  are of the same order of magnitude as found in other systems.<sup>23,24</sup> In summary, the temperature de-

pendence of the conductivity in the metallic phase near the MIT can be described by this model, with parameters that are in reasonable agreement with theoretical predictions.

One final point to be made about the behavior of the conductivity in the critical region of the transition is concerned with the importance of  $e^-e^-$  interactions. In the insulating phase Efros-Shklovskii VRH is observed, suggesting that these interactions are significant. Even as the MIT is approached from the insulating phase the temperature dependence of the conductivity is still consistent with this form of VRH.<sup>21</sup> In the metallic phase the interactions are seen to be important again, while in the critical region the exponent is consistent with the scaling theory with interactions included. All in all,  $e^-e^-$  interactions would appear to play an important role in determining the behavior of the conductivity of  $\text{Cd}_{1-x}\text{Mn}_x\text{Te}:\text{In}$  near the MIT.

#### IV. THE WEAKLY LOCALIZED REGIME (WLR)

The low-temperature transport properties of  $\text{Cd}_{1-x}\text{Mn}_x\text{Te}$  have been studied in the WLR, up to  $\approx 2.5n_c$ . As we shall see in this section, interesting effects occur in some of the samples when the temperature is low enough for the  $s$ - $d$  exchange interaction to dominate over thermal fluctuations. The higher-temperature electrical measurements also show features that are not observed in less conductive samples.

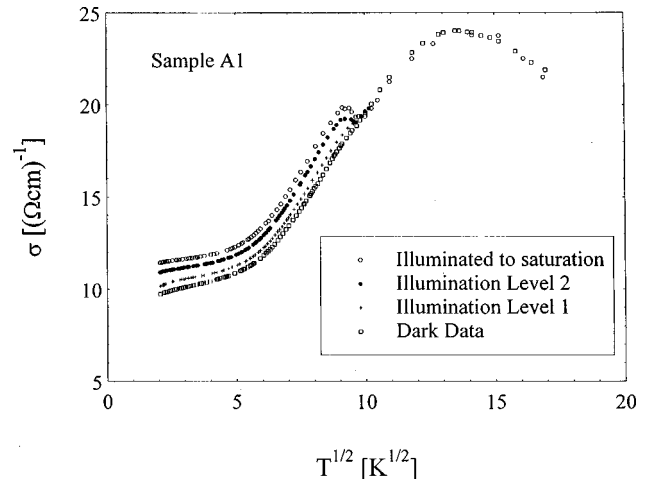


FIG. 5. Temperature dependence of the conductivity from 300 K down to 4.2 K for sample A1. The dark level and three illumination levels are shown.

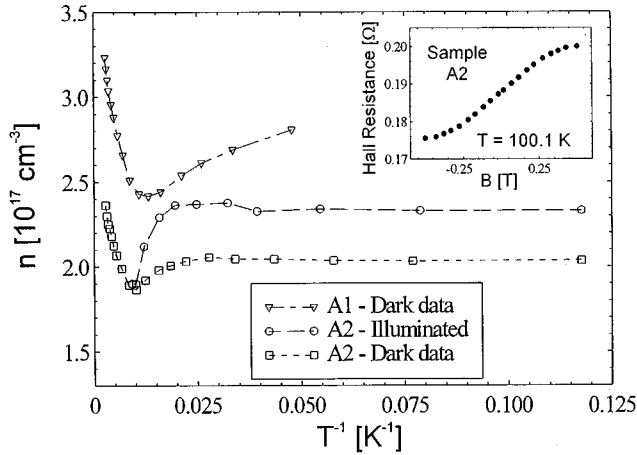


FIG. 6. Temperature dependence of the apparent Hall carrier density of samples A1 and A2. The inset shows the nonlinear Hall effect observed in sample A2 at 100.1 K.

Typical behavior is shown in Figs. 5 and 6, where sample A1 is used as an example. Figure 5 shows the temperature dependence of the conductivity from 300 K down to 4.2 K, for the dark-level and three-photogenerated carrier concentrations. As expected for an  $x=0.047$  sample with  $n \approx 3.0 \times 10^{17} \text{ cm}^{-3}$ , the conductivity is consistent with metallic conduction, i.e., the temperature dependence is weak and  $\sigma(T \rightarrow 0) > 0$ . The temperature dependence of the Hall carrier density for this sample along with that of sample A2 is shown in Fig. 6. Typical behavior is observed with the exception of the “dip” in the apparent carrier density around 70–100 K. At lower temperatures ( $< 60$  K), the carrier density of sample A2 reaches a temperature-independent value, as expected for metallic conduction. It should also be noted that the Hall effect exhibits nonlinearity in this temperature region, whereas at higher and lower temperatures it is linear. The data for sample A2 at 100.1 K are shown in the inset of Fig. 6. This effect is not observed in other less conductive samples<sup>13,14</sup> of  $\text{Cd}_{1-x}\text{Mn}_x\text{Te}:\text{In}$ . This suggests that the anomaly we observe here could be due to the high doping levels required to achieve metallic conduction in samples such as these. Specifically, we propose that the anomaly in the Hall data is due to a crossover from activated conduction from the shallow level to the conduction band at high temperatures ( $> 100$  K) to metallic conduction in the shallow impurity band at lower temperatures. In such a situation one would naturally expect nonlinearity in the Hall voltage in the crossover region. The carrier density of sample A1 would be expected to decrease upon further cooling, eventually reaching a constant value at low temperatures. Unfortunately, it is very difficult to measure the Hall coefficient at lower temperatures than these due to the fact that the positive magnetoresistance effect<sup>20</sup> becomes increasingly large, while the Hall coefficient is relatively small. It should also be noted that the crossover in conduction mechanism occurs at slightly different temperatures for the two samples. This is easily explained in terms of the lower In shallow level activation energy for the sample with lower Mn fraction,<sup>14</sup> although other quantities such as the mobilities in the two bands will have an effect.

The fact that we observe PPC in the metallic phase is worthy of some comment. The PPC effect is due to the ex-

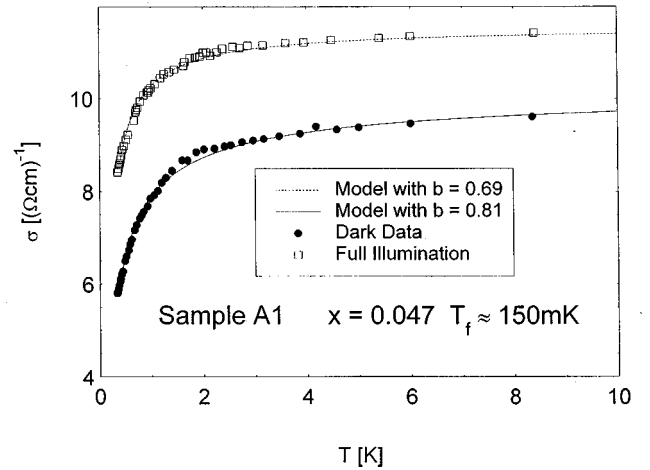


FIG. 7. Temperature dependence of the conductivity of sample A1 from 10 K down to 0.3 K. The dark level and saturation illumination curves are shown. The dotted and solid lines are fits to the model described in the text.

istence of  $DX$  centers, which form deep levels that are highly localized.<sup>9</sup> Naively one might expect that PPC would then be impossible in the metallic phase where the conduction proceeds via extended electronic states. However, it seems clear from the fact that we observe a crossover from activated conduction (from the  $DX$  deep levels) to metallic conduction in an impurity band that the MIT occurs in the impurity band, while the localized states are confined to the  $DX$  deep levels. Hence, the existence of PPC in the metallic phase is to be expected.

The conductivity of the two samples A1 and A2 has been measured down to 335 mK. Figure 7 displays the conductivity of sample A1, while Fig. 8 shows similar data for sample A2. The striking feature observed in both of these measurements is the rapid decrease in the conductivity below a temperature of approximately 1.5–2.0 K. Although this is immediately reminiscent of the data of Dietl *et al.*<sup>15</sup> on BMP scattering in the WLR of  $\text{Cd}_{1-x}\text{Mn}_x\text{Se}:\text{In}$ , it is important to establish that the decrease in conductivity cannot be ex-

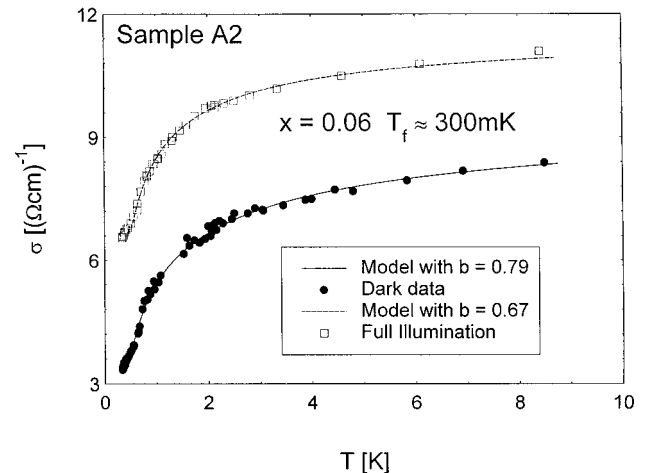


FIG. 8. Temperature dependence of the conductivity of sample A2 from 10 K down to 0.3 K. The dark level and saturation illumination curves are shown. The dotted and solid lines are fits to the model described in the text.

plained naturally by the quantum corrections to the finite zero temperature conductivity. For both sample A1 and sample A2 only a poor fit can be obtained with Eq. (3), while the fitting parameters are clearly unphysical. For example, for sample A1, the fit is restricted to  $T < 0.7$  K, with values such as  $B = 40$ ,  $m = -30$ , and values of  $p$  of around 0.15. It seems clear that the temperature dependence of the conductivity in the WLR is expected to be much weaker than observed here, and that the model that takes into account  $e^-e^-$  interactions and weak localization cannot explain these data.

This leads us to the natural conclusion that we are indeed observing a rapid decrease in the conductivity due to an increased spin-disorder scattering caused by the formation of BMP's on quasilocalized  $s$  spins. This hypothesis can be supported by the results of a simple modeling of the effect. Following Sawicki *et al.*<sup>25</sup> it is possible to model this effect by calculating the effective Bohr radius of the electron around which the polaron forms, from the expression for the free energy of the BMP.<sup>26</sup> Knowing the Bohr radius one can estimate the value of  $n_c$  from the Mott criterion (2) and therefore calculate the zero-temperature conductivity from the scaling relation (1). The expression for the (zero field) free energy of the polaron as given by Dietl<sup>26</sup> is

$$F_p = \frac{\hbar^2}{2m_e^* a_B^2} - \frac{e^2}{\epsilon_0 a_B} - \frac{1}{2} E_p(T), \quad (7)$$

where  $a_B$  is the Bohr radius of the polaron and  $E_p(T)$  is the characteristic energy of the magnetic polaron, given by  $E_p = \alpha^2 \chi(T) / 32 \pi g^2 \mu_B^2 a_B^3$ , where  $\alpha$  is the  $s$ - $d$  exchange energy (0.22 eV for  $\text{Cd}_{1-x}\text{Mn}_x\text{Te}$ ) and  $\chi(T)$  is the macroscopic susceptibility of the system. To obtain the stable Bohr radius of the polaron we minimize Eq. (7) with respect to  $a_B$ . This leads to

$$a_H(T) = \frac{a_H}{2} + \frac{\epsilon}{2e^2} \left[ \frac{\hbar^4}{(m_e^*)^2} - \frac{4e^2}{\epsilon_0} \left( \frac{3\alpha^2 \chi(T)}{64\pi g^2 \mu_B^2} \right) \right]^{1/2}, \quad (8)$$

where  $a_H = \epsilon \hbar^2 / e^2 m_e^*$  is the hydrogenic-theory value for the Bohr radius. At high temperatures where the paramagnetic susceptibility is low, the second term in the square brackets in Eq. (8) is small and the polaron radius tends to the hydrogenic value  $a_H$ . However, at low temperatures the paramagnetic susceptibility can be very large meaning that the second term dominates, and the polaron radius shrinks rapidly, while the binding energy increases. This leads to the efficient spin-disorder scattering of the carriers. Using the Mott criterion (2) and the scaling equation (1) leads to  $\sigma(T) = \sigma_0 (a_B^3 n / 0.0176 - 1)$ , where  $n$  is the carrier density and we take  $v = 1.0$ . This equation allows a calculation of  $\sigma(T)$  in conjunction with Eq. (8). The temperature dependence of the susceptibility at low temperatures has been found to fit the form  $\chi \propto T^{-b}$ , where  $b$  is a constant of the order of 0.7 for  $\text{Cd}_{0.95}\text{Mn}_{0.05}\text{Se}$ :In at  $n/n_c \approx 2.7$ ,<sup>15</sup> The solid lines in Figs. 7 and 8 are fits to this model with  $b$  as a free parameter. As can be clearly seen from the figures, the agreement between this simple model and experiment is good. Moreover, the extracted values of the parameter  $b$  are rather close to the value of 0.7 extracted from an actual measurement of  $\chi(T)$  in  $\text{Cd}_{1-x}\text{Mn}_x\text{Se}$ . The values of the polaron radius estimated

from the conductivity data are also reasonable. For example, for the dark data of sample A1 the polaron radius is roughly constant at 10 nm down to 2 K. Below this the radius decreases rapidly to 9.2 nm at 335 mK. Although these values are large in comparison to the hydrogenic value expected in the insulating phase (5 nm), this might be expected for the case where the polaron forms on a quasilocalized  $s$  spin on the metallic side of the MIT.

It should be noted that this model calculates the effect of the reduction in polaron radius (and hence increase in binding energy) on the zero-temperature conductivity. This behavior will approximate to the actual low-temperature conductivity reasonably well as long as  $n$  is close to  $n_c$ , and the temperature is low enough to approximate the conductivity to the conductivity at absolute zero. It is worth mentioning here that the temperature dependence of the spin-disorder scattering rate due to quasilocalized  $s$  spins, which do not form BMP's, is weakly temperature dependent as it is proportional to  $\chi(T)T$ . This means that the temperature dependence of the conductivity is expected to be weak when BMP formation does not occur. Despite the fact that the model is crude, the agreement between theory and experiment is further evidence for our interpretation of the conductivity data in terms of spin-disorder scattering from BMP's.

One final point to be made about the data of Figs. 7 and 8 is that the polaron scattering begins to dominate the temperature dependence of the conductivity at a higher temperature than observed in  $\text{Cd}_{0.95}\text{Mn}_{0.05}\text{Se}$  ( $\sim 0.5$  K). This temperature is the point at which the spin-disorder scattering rate due to the BMP's begins to dominate over the regular spin-disorder scattering rate due to single Mn ions. This regular spin-disorder scattering rate in the WLR (as given by Dietl *et al.*)<sup>15</sup> can be estimated to be a factor of 2.58 smaller for  $\text{Cd}_{1-x}\text{Mn}_x\text{Te}$  (with these carrier densities) than  $\text{Cd}_{1-x}\text{Mn}_x\text{Se}$ , meaning that the BMP scattering term will dominate at a higher temperature. It should be noted that the differing scattering rates are simply due to the different material parameters involved, along with the lower-carrier densities in  $\text{Cd}_{1-x}\text{Mn}_x\text{Te}$ .

In summary, it seems that sample A1 ( $x = 0.047$ ) and sample A2 ( $x = 0.061$ ) display BMP scattering in the WLR, while sample C5 ( $x = 0.081$ ), which is the sample that can be used to fine-tune the MIT, shows no such behavior. In fact, the transport properties (down to 300 mK) of this sample show no indication of scattering by bound magnetic polarons. In addition to this, there is also the point that the data on the insulating  $x = 0.09$  sample studied by Terry *et al.* indicated that magnetic polaron formation leads to a magnetic hard gap in the density of states.<sup>16</sup> Although this situation would appear to be rather complex, there is a consistent pattern of behavior, the vital point being the paramagnetic to spin-glass transition that is known to occur in these materials.<sup>27</sup> We postulate that the polaron scattering (as observed in samples A1 and A2 and the  $\text{Cd}_{0.95}\text{Mn}_{0.05}\text{Se}$ :In samples of Dietl *et al.* in Ref. 15) is only observable in the paramagnetic phase. The spin-glass freezing temperature ( $T_f$ ) is known to increase rapidly with  $x$ ,<sup>27</sup> meaning that only the samples with low  $x$  values are likely to be in the paramagnetic phase at the temperatures studied here, while samples with higher  $x$  values will show spin-glass ordering. Recent theoretical work has proposed that BMP formation is

profoundly affected by the presence of spin-glass order.<sup>28</sup> Specifically it has been shown that the binding energy of the magnetic polaron tends to a temperature-independent value below the spin-glass freezing temperature. This means that if a sample that has already formed a spin-glass is cooled to low temperatures, no rapid drop in the conductivity will be observed around 1.5 K. The polaron radius and binding energy are temperature independent. Note that Glód *et al.*<sup>29</sup> have also observed a weakening in the low-temperature electrical conductivity of metallic samples of  $\text{Cd}_{1-x}\text{Mn}_x\text{Se}:\text{In}$  and  $\text{Cd}_{1-x}\text{Mn}_x\text{TeSe}:\text{In}$ . The authors interpret their data as resulting from the scattering of electrons by bound magnetic polarons, but with a weakened temperature dependence arising from the form of the magnetic susceptibility of the materials in question in the spin-glass phase.

The existing data on the  $x$  dependence of  $T_f$  (Refs. 27 and 30) can be used to estimate the spin-glass freezing temperature of the sample studied here. We find  $T_f \approx 150$  mK for sample A1, suggesting that this sample is in the paramagnetic phase down to 300 mK. This is consistent with the observation of the onset of BMP scattering in this sample. For sample A2,  $T_f \approx 300$  mK, suggesting that spin-glass ordering will only occur at the lowest temperatures studied. Again, this is consistent with the observed BMP scattering. In addition to this, it also explains the weakening of the temperature dependence of the conductivity below about 400 mK for sample A2. This is due to the onset of spin-glass ordering in this sample. It should be noted that this effect is also visible in the data of Dietl *et al.*<sup>15</sup> on  $\text{Cd}_{0.95}\text{Mn}_{0.05}\text{Se}:\text{In}$  at a temperature of around 110 mK. The temperature dependence of the susceptibility of this sample was measured in this temperature region and showed a paramagnetic to spin-glass transition at 95 mK, suggesting that these data are in agreement with our model.

Evidence for the theoretical prediction that the binding energy of the magnetic polaron is weakly temperature dependent in the spin-glass phase is given by the transport data of Terry *et al.*<sup>16</sup> on the insulating sample of  $\text{Cd}_{0.91}\text{Mn}_{0.09}\text{Te}:\text{In}$ . As mentioned earlier this sample exhibits a crossover from Efros-Shklovskii VRH to a temperature dependence of the resistivity of the form  $\exp(E_H/k_B T)$  as the carrier density is increased. This was interpreted in terms of the existence of a hard gap in the density of states due to BMP formation on shallow In donors. The important point here is that the data of Ref. 16 are very linear in  $\ln \sigma$  against  $T^{-1}$  suggesting that the hard-gap energy  $E_H$  (and therefore the binding energy) is temperature independent. This is consistent with the lack of temperature dependence of the BMP binding energy. The behavior of sample C5 can also be understood within this model. Although  $T_f \approx 0.6$  K the VRH conduction near the MIT shows no evidence for the formation of BMP's due to the fact that the hard gap in the density of states is likely to form at lower temperatures than those used in this study. This is a consequence of the higher-carrier densities in this sample, which will result in BMP's with a large radius and a small binding energy, which will have no effect on the conduction in this sample.

One final test of our model would be to measure the temperature dependence of the conductivity of a sample with a large  $x$  value at low temperatures. This is normally impossible as the high- $x$  samples are generally very insulating due

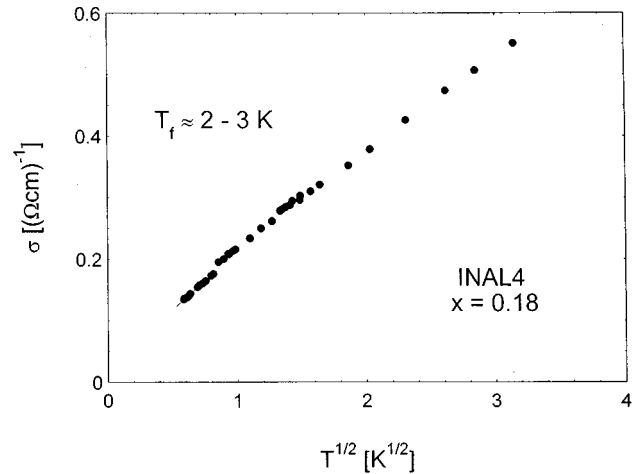


FIG. 9. Temperature dependence of the conductivity of sample INAL4 from 10 K down to 0.3 K. The solid line is a fit to the low-temperature data using Eq. (3) with the parameters shown in the text.

to the large deep-level activation energy<sup>14</sup> lowering the density of free carriers. However, doping  $\text{Cd}_{1-x}\text{Mn}_x\text{Te}$  with In and Al results in persistent photoconductors with large carrier densities, even at high  $x$  (15–20 %). This is possible because although Al forms a  $DX$  center in this material, the deep level is not in the forbidden gap (at least not at these Mn concentrations),<sup>31</sup> meaning that all of the Al-dopant atoms result in shallow  $n$ -type doping. Figure 9 shows the temperature dependence of the conductivity of a sample of  $\text{Cd}_{0.82}\text{Mn}_{0.18}\text{Te}:\text{In}, \text{Al}$  with a carrier density of  $3.98 \times 10^{17} \text{ cm}^{-3}$  at 300 K. A sample with this  $x$  value would be expected to undergo a transition from the paramagnetic phase to the spin-glass phase at  $T_f \sim 2\text{--}3$  K. As can be clearly seen from Fig. 9, the temperature dependence of the conductivity differs from that seen in samples A1 and A2 in that no dramatic decrease in the conductivity occurs. This provides further support for the hypothesis that the binding energy of the magnetic polaron is weakly temperature dependent in the spin-glass phase.

Another interesting point can be made about the data of Fig. 9, in that the temperature dependence of the conductivity is quantitatively different to that observed in the sample used to tune the MIT. Examination of the figure shows that the low-temperature conductivity would appear to be linear in  $T^{1/2}$ , suggesting that  $e^-e^-$  interactions alone dominate the conductivity. A fit to the data with Eq. (3) is shown by the dotted line in Fig. 9. This fit results in the values  $\sigma(T=0) = 0.015 (\Omega \text{cm})^{-1}$ ,  $m = 0.281 (\Omega \text{cm K}^{1/2})^{-1}$ , and  $B = -0.025 (\Omega \text{cm K})^{-1}$ . The remarkable point about these parameters is that the magnitude of  $B$  is close to zero: it is in fact over  $10^2$  times smaller than the largest value of  $B$  recorded for the other samples. This would certainly seem to suggest that the weak localization effect is not present in this sample. We suggest that this is due to the increased density of magnetic ions in this sample ( $x = 0.18$  compared to  $x = 0.08$  for the other sample). The weak localization effect comes about due to interference of coherent electronic wave functions that leads to an effective localization of the electrons.<sup>32</sup> This wave-function coherence is lost in the presence of magnetic atoms or when a weak magnetic field is



applied, leading to the characteristic negative magnetoresistance observed in this regime.<sup>32</sup> It therefore seems reasonable to expect that scattering off magnetic ions such as Mn in  $\text{Cd}_{1-x}\text{Mn}_x\text{Te}$  may lead to a suppression of the weak localization effect. Thus, we propose that the absence of weak localization effects in the  $x=0.18$  sample may be due to this suppression of weak localization because of the increased density of magnetic ions. It should be noted that the observed value of  $m$  for this sample is consistent with the data on doped  $\text{Si}^{24}$  where  $m(n)$  undergoes a change in sign very close to the MIT, as well as being of the same order of magnitude as found in  $\text{Al}_x\text{Ga}_{1-x}\text{As}:\text{Si}$ .<sup>10</sup>

## V. SUMMARY AND CONCLUSIONS

This paper has presented comprehensive data on the temperature dependence of the conductivity in the metallic phase of  $\text{Cd}_{1-x}\text{Mn}_x\text{Te}$  near the MIT. We have studied the critical region of the MIT using the persistent photoconductivity effect displayed by this diluted magnetic semiconductor. This has allowed us to fine-tune the MIT by illumination in zero magnetic field, and has led to the first determination of the critical exponent of the transition in a magnetic system in zero magnetic field. In fact, to our knowledge, persistent photoconductivity has only been used once previously to study the MIT.<sup>10</sup> We obtain  $n_c=2.34\times 10^{17}\text{ cm}^{-3}$ ,  $\sigma_0=3.57(\Omega\text{ cm})^{-1}$ , and  $\nu\approx 1.0$ , for  $x=0.08$ . The critical carrier density is in agreement with past work in the insulating phase, while the exponent is the same as that determined in other magnetic semiconductors. An exponent of 1 is also in

agreement with the scaling theory with interactions included as well as a large body of experimental evidence on compensated semiconductors. The temperature dependence of the metallic conductivity in the vicinity of the transition has been satisfactorily explained by a model that takes into account  $e^-e^-$  interactions and weak localization. The importance of  $e^-e^-$  interactions near the MIT have been stressed. In the weakly localized regime the temperature dependence of the conductivity of some samples shows a dramatic decrease in the conductivity when the temperature is low enough for the  $s$ - $d$  exchange interaction to dominate. This exchange interaction leads to the formation of bound magnetic polarons, which result in efficient spin-disorder scattering at low temperatures. Other samples with higher Mn content do not show this effect. We interpret this situation as evidence for the recent theoretical speculation that the binding energy of the magnetic polaron is weakly temperature dependent in the spin-glass phase. This leads us to suggest that electron scattering by bound magnetic polarons can only be unambiguously observed in the paramagnetic phase of dilute magnetic semiconductors. Hence low  $x$  samples with low spin-glass freezing temperatures should exhibit a strongly temperature-dependent electrical conductivity describable by bound magnetic-polaron scattering for  $T\geq T_f$ . However, samples with higher  $x$  values enter the spin-glass ordered phase at a temperature where no dramatic decreases in the conductivity arising from BMP scattering can be observed. This model satisfactorily explains all of the available data, including that on  $\text{Cd}_{1-x}\text{Mn}_x\text{Se}$ .<sup>15</sup>

- 
- <sup>1</sup>E. Abrahams, P. W. Anderson, D. C. Licciardello, and T. V. Ramakrishnan, *Phys. Rev. Lett.* **42**, 673 (1979).  
<sup>2</sup>P. W. Anderson, *Phys. Rev.* **109**, 1492 (1958).  
<sup>3</sup>T. F. Rosenbaum, K. Andres, G. A. Thomas, and R. N. Bhatt, *Phys. Rev. Lett.* **43**, 1723 (1980).  
<sup>4</sup>W. N. Shafarman, D. W. Koon, and T. G. Castner, *Phys. Rev. B* **40**, 1216 (1989).  
<sup>5</sup>A. N. Ionov, M. J. Lea, and R. Rentzsch, *Pis'ma Zh. Eksp. Teor. Fiz.* **54**, 470 (1991) [*JETP Lett.* **54**, 473 (1991)].  
<sup>6</sup>W. Sasaki, in *Anderson Localization*, edited by T. Ando and H. Fukuyama (Springer-Verlag, Berlin, 1987) p. 10.  
<sup>7</sup>D. Belitz and T. R. Kirkpatrick, *Rev. Mod. Phys.* **66**, 261 (1994).  
<sup>8</sup>M. A. Paalanen, T. F. Rosenbaum, G. A. Thomas, and R. N. Bhatt, *Phys. Rev. Lett.* **48**, 1284 (1982).  
<sup>9</sup>For a review see P. M. Mooney, *J. Appl. Phys.* **67**, R1 (1990).  
<sup>10</sup>S. Katsumoto, in *Anderson Localization* (Ref. 6), p. 45.  
<sup>11</sup>S. von Molnar, A. Briggs, J. Flouquet, and G. Remenyi, *Phys. Rev. Lett.* **51**, 706 (1983).  
<sup>12</sup>T. Wojtowicz, T. Dietl, M. Sawicki, W. Pleisewicz, and J. Jaroszynski, *Phys. Rev. Lett.* **56**, 2419 (1986).  
<sup>13</sup>I. Terry, T. Penney, S. von Molnar, J. M. Rigotty, and P. Becla, *Solid State Commun.* **84**, 235 (1992).  
<sup>14</sup>C. Leighton, I. Terry, and P. Becla, *Phys. Rev. B* **56**, 6689 (1997).  
<sup>15</sup>T. Dietl, M. Sawicki, T. Wojtowicz, J. Jaroszynski, W. Pleisewicz, L. Swierkowski, and J. Kossut, in *Anderson Localization* (Ref. 6), p. 58.  
<sup>16</sup>I. Terry, T. Penney, S. von Molnar, and P. Becla, *Phys. Rev. Lett.* **69**, 1800 (1992).  
<sup>17</sup>I. Terry, T. Penney, S. von Molnar, and P. Becla, *J. Cryst. Growth* **159**, 1070 (1996).  
<sup>18</sup>T. Wojtowicz, S. Kolesnik, I. Miotkowski, and J. K. Furdyna, *Phys. Rev. Lett.* **70**, 2317 (1993).  
<sup>19</sup>N. F. Mott, *Conduction in Non-Crystalline Materials* (Oxford Science, Oxford, 1987).  
<sup>20</sup>Y. Shapira, N. F. Oliveira, Jr, P. Becla, and T. Q. Vu, *Phys. Rev. B* **41**, 5931 (1990).  
<sup>21</sup>C. Leighton, I. Terry, and P. Becla, *Europhys. Lett.* **42**, 67 (1998).  
<sup>22</sup>P. A. Lee and T. V. Ramakrishnan, *Rev. Mod. Phys.* **57**, 287 (1985).  
<sup>23</sup>G. A. Thomas, A. Kawabata, Y. Ootuka, S. Katsumoto, S. Kobayashi, and W. Sasaki, *Phys. Rev. B* **26**, 2113 (1982).  
<sup>24</sup>P. Dai, Y. Zhang, and M. P. Sarachik, *Phys. Rev. B* **45**, 3984 (1992).  
<sup>25</sup>M. Sawicki, T. Dietl, J. Kossut, J. Igalson, T. Wojtowicz, and W. Pleisewicz, *Phys. Rev. Lett.* **56**, 508 (1986).  
<sup>26</sup>T. Dietl, in *Handbook on Semiconductors*, edited by T. S. Moss (Elsevier, New York, 1994), Vol. 3, p. 1291.  
<sup>27</sup>S. Oseroff and P. H. Keesom, in *Diluted Magnetic Semiconductors*, edited by J. K. Furdyna and J. Kossut, *Semiconductors and Semimetals* vol. 25 (Academic, New York, 1988) p. 75.  
<sup>28</sup>A. L. Chudnovskiy, R. Oppermann, B. Rosenow, P. R. Yakovlev, U. Zehnder, and W. Ossau, *Phys. Rev. B* **55**, 10 519 (1997).  
<sup>29</sup>P. Glód, T. Dietl, M. Sawicki, and I. Miotkowski, *Physica B* **194-196**, 995 (1994); P. Glód, T. Dietl, T. Wojtowicz and M. Sawicki, *Acta Phys. Pol. A* **84**, 657 (1993).

<sup>30</sup>J. Kossut and W. Dobrowolski, in *Handbook of Magnetic Materials*, edited by K. H. J. Buschow (Elsevier, New York, 1993).

<sup>31</sup>Al doping is likely to result in PPC in  $\text{Cd}_{1-x}\text{Mn}_x\text{Te}$  at much higher Mn concentrations than these. This is elucidated by the

pressure dependence study of doping in CdTe by G. W. Iseler, J. A. Kafalas, A. J. Strauss, H. F. MacMillan, and R. H. Bube, *Solid State Commun.* **10**, 619 (1972).

<sup>32</sup>G. Bergmann, *Phys. Rep.* **107**, 1 (1984).